Rapid Communications

Double-mode relaxation of highly deformed anisotropic vesicles

Dinesh Kumar,[1,2] Channing M. Richter,[1] and Charles M. Schroeder[1,2,3,*]

[1]*Department of Chemical and Biomolecular Engineering, University of Illinois at Urbana-Champaign, Urbana, Illinois 61801, USA*
[2]*Beckman Institute for Advanced Science and Technology, University of Illinois at Urbana-Champaign, Urbana, Illinois 61801, USA*
[3]*Department of Materials Science and Engineering, University of Illinois at Urbana-Champaign, Urbana, Illinois 61801, USA*

(Received 27 February 2020; accepted 17 June 2020; published 7 July 2020)

Lipid vesicles are known to undergo complex conformational transitions, but it remains challenging to systematically characterize nonequilibrium membrane dynamics in flow. Here, we report the direct observation of anisotropic vesicle relaxation from highly deformed shapes using a Stokes trap. Vesicle shape relaxation is described by two distinct characteristic timescales governed by the bending modulus and membrane tension. Interestingly, the fast double-mode timescale is found to depend on vesicle deflation or reduced volume. Experimental results are well described by a viscoelastic model of a deformed membrane. Overall, these results show that vesicle relaxation is governed by an interplay between membrane elastic moduli, surface tension, and vesicle deflation.

DOI: 10.1103/PhysRevE.102.010605

Membrane-bound vesicles are ubiquitous in biological systems [1,2] and drug delivery applications [3]. Phospholipid vesicles are often used as model systems to study the mechanical properties of living cells [4–10]. In addition, synthetic vesicles serve as triggered-release agents [11] or encapsulants in detergents and fabric softeners [12]. In many cases, structure-property relations underlie the functional behavior of these materials. Despite recent progress, however, the nonequilibrium shape dynamics of highly deflated vesicles is not yet fully understood [13–18].

Vesicles undergo a wide array of stretching dynamics in flow depending on the flow type and equilibrium vesicle shape [19–24]. In shear flow, vesicles exhibit tumbling, tank-treading, and membrane trembling behavior that depends on the flow strength and viscosity ratio [18,19,25]. In extensional flow, vesicles with nonspherical equilibrium shapes exhibit a wide array of conformational transitions, including a tubular-to-symmetric dumbbell transition for highly deflated vesicles [20,23,26,27], a spheroidal-to-asymmetric dumbbell transition for moderately deflated vesicles [22,23,26], and a nearly spherical-to-ellipsoidal transition for weakly deflated vesicles [23,28–31]. Such deformable membrane behavior is naturally exploited in biological systems; for example, red blood cells readily adopt biconcave disk shapes [32], enabling large reversible deformation while traversing thin capillaries during circulation.

Vesicle relaxation following deformation is critically important for shape dynamics and reversible elastic behavior [6]. Prior work has focused on the near-equilibrium relaxation of quasispherical vesicles following small deformations, induced by relatively weak forces using optical tweezers [30] or electrodeformation [33]. Kantsler *et al.* [20] observed the relaxation of a weakly deformed tubular-shaped vesicle, albeit only for a small ensemble size. Broadly, fundamental studies of shape relaxation for freely suspended vesicles following large nonlinear deformations are challenging due to the need for precise flow control and manipulation without using micropipettes or direct physical contact of membranes.

Here, we report the direct observation of anisotropic vesicle relaxation following large nonlinear deformations in extensional flow. Vesicles with nonspherical shapes at equilibrium are deformed in precisely controlled flows using a Stokes trap [34–37], followed by relaxation under quiescent conditions. Remarkably, our results show that highly deformed, freely suspended anisotropic vesicles relax by a double-mode exponential pathway governed by two distinct and well-separated timescales corresponding to characteristic bending and surface tension timescales.

Giant unilamellar vesicles (GUVs) are prepared from a mixture of 1,2-dioleoyl-sn-glycero-3-phosphocholine (DOPC) and 0.12 mol % of the fluorescent lipid 1,2-dioleoyl-sn-glycero-3-phosphoethanolamine-*N*-(lissamine rhodamine B sulfonyl) in 100 mM sucrose buffer using an electroformation method (Supplemental Material [38]) [23,39]. Following electroformation, GUVs are slightly deflated by introducing a higher osmolarity sucrose solution to the outer fluid. Deflated vesicles are described by a reduced volume $v = (3V\sqrt{4\pi})/A^{3/2}$, where V and A are the equilibrium vesicle volume and surface area, respectively, determined by revolution of the membrane contour, as previously described [22,23]. In this way, v is a measure of vesicle anisotropy, such that $v = 1$ corresponds to a perfectly spherical shape.

Prior to vesicle stretching experiments, we determined the average bending modulus of quasispherical vesicles to be $\kappa = 22.3k_BT$ using fluctuation spectroscopy, as previously described [23,40,41]. In all subsequent experiments, vesicles are deformed in the bending-dominated regime, such that no area stretching of the membrane occurs in the initial stretching step prior to vesicle relaxation (Supplemental Material [38]). The crossover tension from the bending to the area stretching

*cms@illinois.edu

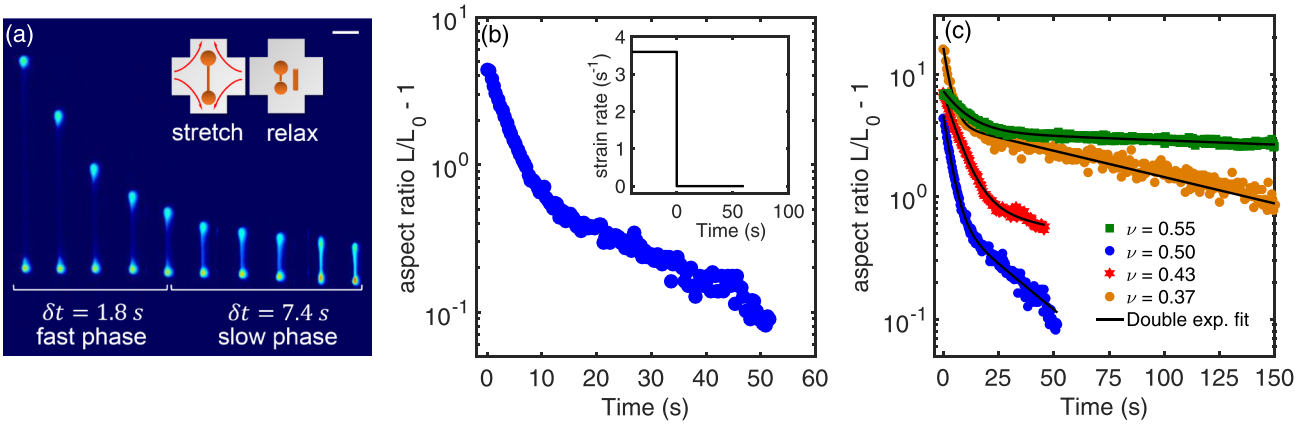

FIG. 1. Relaxation of highly deformed anisotropic vesicles using a Stokes trap. (a) Time series of images showing a vesicle ($\nu = 0.5$) relaxing back to an equilibrium tubular shape after being deformed into a symmetric dumbbell in extensional flow. Time between snapshots is $\delta t = 1.8$ s for the fast phase and 7.4 s for the slow phase. Scale bar is 20 μm. (b) Time trajectory of vesicle shape relaxation following deformation in flow, showing a semilogarithmic plot of the aspect ratio $L/L_0 - 1$ as a function of time for the vesicle in Fig. 1(a). Inset: Flow deformation protocol prior to vesicle relaxation. At time $t = 0$, the flow is stopped and the membrane relaxes back to equilibrium. (c) Semilogarithmic plot of the aspect ratio $L/L_0 - 1$ as a function of time for different vesicles having reduced volume $\nu = 0.55, 0.5, 0.43, 0.37$ with corresponding double-exponential fits.

regime is given by $\sigma = K_a k_B T/8\pi\kappa \approx 0.1$ mN/m [42,43], where K_a is the area-stretching modulus, k_B is the Boltzmann constant, T is absolute temperature, and κ is the bending modulus. In our experiments, the maximum membrane tension is typically one order of magnitude smaller than the crossover tension (Supplemental Material [38], Table S1).

We began by studying the conformational relaxation of nearly spherical vesicles ($\nu > 0.9$) using the Stokes trap. Quasispherical vesicles ($\nu = 0.95$) retain an ellipsoidal shape in extensional flow without transitioning into a dumbbell shape (Supplemental Material [38], Fig. S1) [23,30,31,33]. Following cessation of flow, nearly spherical vesicles undergo a rapid initial retraction (first few images in Fig. S1 [38]) that occurs at a rate slightly slower than the sampling rate of the imaging system (Supplemental Material [38]). The rapid initial retraction is followed by a slow relaxation response that is well described by a single exponential decay, as shown in Fig. S2 [38]. Overall, these observations for quasispherical vesicles are consistent with prior electrodeformation experiments [33] and theoretical predictions [44,45]. Based on these results, we hypothesized that highly deflated vesicles may exhibit a double-mode relaxation process that would show longer timescale dynamics compared to nearly spherical vesicles. However, to our knowledge, systematic experimental characterization of vesicle relaxation dynamics following large nonlinear deformation for the broad range of reduced volume $0.2 < \nu < 0.95$ has not been previously reported.

We next characterized the transient relaxation dynamics of deflated vesicles with reduced volumes $\nu < 0.75$ (Fig. 1). Here, vesicles are deformed in extensional flow using strain rates $\dot{\epsilon}$ larger than the critical strain rate $\dot{\epsilon}_c$ required for shape deformation for floppy vesicles [23]. Using the Stokes trap, vesicles are deformed in flow for $\approx$40 s, thereby generating large accumulated fluid strains $\epsilon = \dot{\epsilon}t = 40$–$400$ and achieving vesicle aspect ratios $L/L_0 \approx 4$–16, where L is the vesicle stretch along the axis of extension and L_0 is the vesicle extension at equilibrium in the absence of flow. During the deformation step ($\dot{\epsilon} > \dot{\epsilon}_c$), a vesicle undergoes a nonequilibrium shape transition into a symmetric dumbbell for $0.25 < \nu < 0.60$ [Fig. 1(a), Supplemental Material Movie 1] or an asymmetric dumbbell for $0.60 < \nu < 0.75$ with a long, thin tether [23]. Following deformation, the flow field is abruptly stopped, and vesicles relax back to an equilibrium shape under quiescent conditions (Supplemental Material [38], Fig. S3). Experiments are performed for vesicles located near the center plane of the microdevice in the vertical direction, such that the strain rate is well characterized using particle tracking velocimetry as previously reported [23].

A characteristic transient relaxation trajectory for a highly deformed vesicle ($\nu = 0.5$) is shown in Fig. 1(b), with the time series of images shown in Fig. 1(a). Prior to flow cessation, the vesicle deforms into a symmetric dumbbell with a long, thin tether connecting the two spherical ends [Fig. 1(a)]. Following flow cessation, the vesicle eventually relaxes back to its equilibrium shape. The transient relaxation trajectory reveals that vesicle shape relaxes via two stages: an initial fast retraction step, where the length of thin tether rapidly shortens, followed by a slow relaxation step in which the vesicle returns to an equilibrium shape.

A series of characteristic relaxation trajectories for vesicles with different reduced volumes ν is shown in Fig. 1(c) (Supplemental Material [38], Fig. S4), where the vesicle aspect ratio is defined by $L(t)/L_0 - 1$, and $L(t)$ is the time-dependent vesicle extension along the elongational axis. In all cases, our results show that the vesicle relaxation trajectories can be described by a double-mode exponential decay across a wide range of reduced volumes [Fig. 1(c)]:

$$\frac{L(t)}{L_0} - 1 = A\exp(-t/\tau_1) + B\exp(-t/\tau_2), \qquad (1)$$

where τ_1 and τ_2 are the fast and slow relaxation times, respectively, and A and B are numerical constants. Repeated relaxation experiments on the same vesicle show nearly identical relaxation trajectories (Supplemental Material [38],

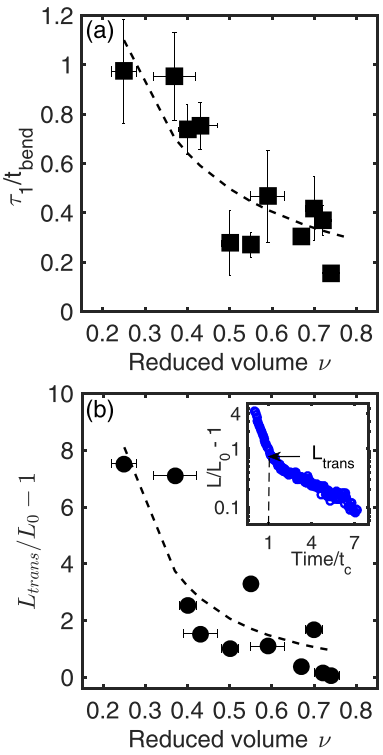

FIG. 2. Characterization of the fast double-mode relaxation time τ_1. (a) Normalized timescale τ_1/t_{bend} as a function of reduced volume ν. The dashed line is a guide for the eye. (b) Transition aspect ratio $L_{\text{trans}}/L_0 - 1$ at the crossover time t_c between the fast and slow relaxation phases as a function of reduced volume ν. Inset: A representative relaxation trajectory for $\nu = 0.5$ showing L_{trans} at crossover time t_c. The dashed line is a guide for the eye.

Fig. S5), which is consistent with the notion that the ratio of thermal energy to the bending modulus $k_BT/\kappa \approx 0.04$ is small, suggesting that vesicle shape relaxation governed by membrane bending fluctuations is nearly deterministic under repeated relaxation trials.

We determined the double-mode relaxation times τ_1 and τ_2 for vesicles over a wide range of reduced volumes ($0.25 < \nu < 0.75$), as shown in Fig. 1(c) (Supplemental Material [38], Fig. S4, Table S1). Interestingly, the numerical values of the fast relaxation time τ_1 are on the order of the characteristic bending relaxation time $t_{\text{bend}} = \mu R^3/\kappa$, where μ is the viscosity of suspending medium and R is the equivalent radius of a vesicle determined from $R = \sqrt{(A/4\pi)}$ [Fig. 2(a)]. Here, the timescale t_{bend} corresponds to the leading order time constant for the longest bending mode, but other fluctuation modes exist in the full spectrum [46]. These results suggest that τ_1 corresponds to relaxation of long-wavelength bending modes following a nonlinear membrane deformation. Interestingly, repeated relaxation trials on the same vesicle show that τ_1 does not depend on the strain rate used in the deformation step (Supplemental Material [38], Table S2 and Fig. S6), which is consistent with the notion that vesicles are deformed in the bending-dominated regime with no significant changes in the membrane structure.

Despite the apparent similarity to the bending relaxation time t_{bend}, unexpectedly, our data show that the normalized fast double-mode relaxation time τ_1/t_{bend} is a function of the vesicle reduced volume ν, as shown in Fig. 2(a). In particular, the normalized fast retraction time τ_1/t_{bend} decreases as the reduced volume increases, which is consistent with the fact that vesicles with smaller reduced volumes have larger surface area to volume ratios and hence larger degrees of membrane floppiness. In Fig. 2, error bars for reduced volume arise from measurement uncertainty in the vesicle equivalent radius R, propagated from vesicle surface area A and volume V, as previously described [23].

Following the initial fast relaxation step, the vesicle membrane transitions to a slow relaxation process described by a second timescale τ_2. Interestingly, the numerical values of τ_2 are on the order of the characteristic surface tension timescale $t_{\text{surf}} = \mu L_{\text{trans}}/\sigma_0$ (Supplemental Material [38], Fig. S7), where σ_0 is the ensemble-averaged equilibrium tension [23] and L_{trans} is the vesicle stretch at the crossover time between the fast and slow regimes, defined as $t_c = C\tau_1\tau_2/(\tau_2 - \tau_1)$ from Eq. (1), where $C = \ln B/A$. In particular, our results show that τ_2 is within an order of magnitude of t_{surf}, which is consistent with the relatively broad distribution of membrane tensions known to result from generating vesicles using electroformation [22,23,33]. Here, the membrane tension for any single vesicle may vary by an order of magnitude around the mean value σ_0 for the ensemble. Overall, the slow mode described by t_{surf} is analogous to the relaxation of Newtonian fluid drops following deformation in flow, where a constant surface tension drives the drop back to its equilibrium spherical shape [47].

Interestingly, our results further show that the vesicle aspect ratio at the transition between the fast and slow relaxation phases ($L_{\text{trans}}/L_0 - 1$) is a function of reduced volume [Fig. 2(b)]. These results suggest that the bending modulus κ may have a functional dependence on the reduced volume ν. Broadly, these findings might have origins in more subtle aspects of membrane mechanics of deflated anisotropic vesicles. Deflated vesicles are known to exhibit an imbalance in lipid density in the two leaflets of the membrane that induces a spontaneous curvature generation [48]. Such modification of the spontaneous curvature and high lateral diffusion of individual lipid molecules in the bilayer for vesicles with smaller reduced volumes may reduce the energy requirements for thermal fluctuations, thereby resulting in a dependence of bending modulus on the degree of osmotic deflation, similar to the observed decrease in bending modulus accompanied by enhanced thermal fluctuations in DOPC bilayers by insertion of an external molecule [49]. Finally, relaxation of highly deformed vesicles with a dumbbell shape involves fluid flow through the thin tether connecting the bulbs. Resistance to flow through the thin tether introduces an additional timescale $\mu L_{\text{max}}^2 R_v/\sigma_0 r_t^2$, where R_v is the radius of the spherical bulb consuming the thin tether, and r_t is the tether radius at the beginning of relaxation. For our experiments, this timescale is several orders of magnitude larger than τ_1 and τ_2, suggesting that bending fluctuations and surface tension drive the conformation relaxation of deformed vesicles.

Viscoelastic models are widely used to characterize the rheological properties of soft materials such as polymers, tissues, and spherical cell aggregates [50–52]. Although bulk rheological measurements of vesicles could be used to

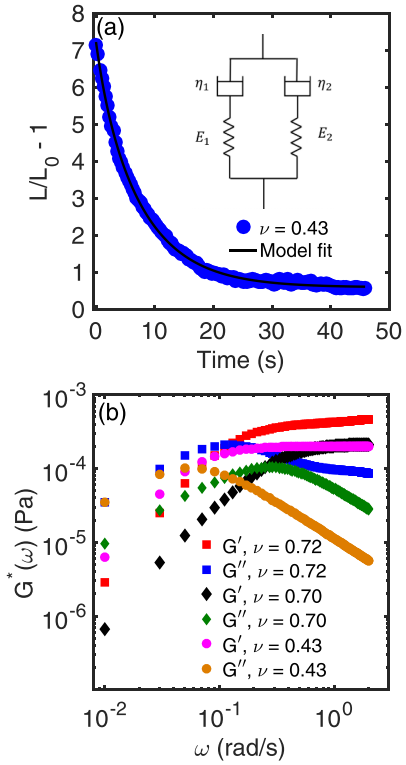

FIG. 3. Viscoelastic model for vesicle membranes. (a) Fit of viscoelastic model to representative relaxation trajectory for vesicle with reduced volume $\nu = 0.43$. (b) Viscoelastic model predictions of storage $G^*(\omega)$ and loss $G''(\omega)$ moduli for three different reduced volumes.

determine the dynamic elastic and viscous modulus of these materials, such experiments are challenging due to sample polydispersity. Here, we present a simple mechanical model which describes the viscoelastic properties of single isolated vesicles over a wide range of frequencies and large deformations. In particular, the double-mode relaxation behavior of a vesicle membrane can be described by a viscoelastic model consisting of two Maxwell elements in a parallel arrangement with moduli (E_1, E_2) and viscosities (η_1, η_2) (Fig. 3 and Supplemental Material [38]). Experimental data on vesicle relaxation is well described by the two-mode viscoelastic model, as shown in Fig. 3(a), thereby enabling determination of the model parameters E_1, E_2, η_1, and η_2. Using the model and parameters determined by fitting to experimental data, the frequency-dependent complex shear modulus $G^*(\omega)$ can be determined. In particular, the storage modulus $G'(\omega)$ and the loss modulus $G''(\omega)$ can be obtained for single vesicles (Supplemental Material [38]) [53]:

$$G'(\omega) = \frac{E_1\left(\omega\frac{\eta_1}{E_1}\right)^2}{1+\left(\omega\frac{\eta_1}{E_1}\right)^2} + \frac{E_2\left(\omega\frac{\eta_2}{E_2}\right)^2}{1+\left(\omega\frac{\eta_2}{E_2}\right)^2}, \tag{2}$$

$$G''(\omega) = \frac{E_1\omega\frac{\eta_1}{E_1}}{1+\left(\omega\frac{\eta_1}{E_1}\right)^2} + \frac{E_2\omega\frac{\eta_2}{E_2}}{1+\left(\omega\frac{\eta_2}{E_2}\right)^2}, \tag{3}$$

where ω is the deformation frequency.

Plots of $G'(\omega)$ and $G''(\omega)$ for vesicles with different reduced volumes are shown in Fig. 3(b). Results from model predictions show that the elastic modulus $G'(\omega)$ increases with frequency and becomes larger than the viscous modulus $G''(\omega)$ at a crossover frequency corresponding to the fast timescale τ_1, which is a signature of a transition from fluid to solidlike behavior. Moreover, the model predicts an approximate plateau modulus $G_0 \approx 10^{-4}$ Pa [Fig. 3(b)], which has not been previously reported for lipid vesicles in the literature.

The parameters from the micromechanical model can be related to membrane physical properties. Interestingly, the model yields a value of $\eta_1 \approx 10^{-3}$ Pa s, which is order-of-magnitude consistent with the solution viscosity in our experiments. The values of η_2 obtained from the model range between 10^{-4} and 10^{-3} Pa s for different vesicles in the ensemble. Assuming a membrane thickness of 5 nm, values of η_2 correspond to a membrane viscosity of 10^{-13}–10^{-12} Pa s m, which are three orders of magnitude lower than the membrane viscosity of spherical DOPC lipid vesicles measured from rotational and translational diffusion probes [54]. However, our work focuses on nonspherical deflated vesicles, which are qualitatively different than spherical vesicles. In particular, the availability of large excess area and higher lateral diffusion of individual lipid molecules in the bilayer membrane are consistent with a decrease in the membrane viscosity. From this perspective, we posit that the values of η_1 and η_2 from the micromechanical model correspond to the solution viscosity and membrane viscosity, respectively.

We further consider the moduli E_1 and E_2 obtained from applying the micromechanical model to our experimental data. The value of E_1 was determined to be $\approx 10^{-4}$ Pa, whereas the value of E_2 ranges between 10^{-4} and 10^{-3} Pa. For a typical vesicle size of $R = 10$ μm, we can estimate the membrane bending modulus from the relation $\kappa \approx E_1 R^3$, yielding $\kappa \approx 10^{-19}$ J, which is in good agreement with the bending modulus measured for DOPC lipid vesicles in our work ($\kappa = 22.3 k_B T$) [23]. Similarly, the surface tension $\sigma \approx E_2 R$ of vesicles varies between 10^{-9} and 10^{-8} N/m, which is consistent with the values determined at equilibrium using fluctuation spectroscopy [23]. While a complete viscoelastic model would relate the physical parameters E_1, E_2, η_1, η_2 to bending modulus, tension, and medium viscosity, the broad variety of equilibrium shapes (e.g., tubular, discoid, spheroid) of deflated vesicles generally complicates analytical modeling, as the base state is perturbed far from a spherical geometry [52,55]. Numerical simulations could be used to characterize the dynamic frequency-dependent rheological properties of lipid vesicles and polymersomes following high deformation.

In this Rapid Communication, we directly observe the relaxation of highly deformed vesicles in quiescent solution. Our results show that vesicles dissipate stress via two distinct and well-separated timescales, with a fast and a slow timescale attributed to the relaxation of bending fluctuation modes and surface tension–dominated modes, respectively. Broadly speaking, these results show how the interplay between vesicle reduced volume, bending forces, and surface tension yields a complex relaxation behavior that has not been previously observed in tethers extruded from quasispherical vesicles [56,57]. These results highlight the use of the

Stokes trap in observing the dynamic behavior of vesicle shape relaxation following deformation in strong flows. This methodology of combining gentle flow-based trapping with fluorescence microscopy to induce large membrane deformation will open new avenues in understanding the dynamics of other membrane-bound particles such as polymersomes, capsules, and living cells without the need for micropipettes or external manipulation of membranes.

We thank Noah Hopkins for assistance in analyzing experimental data. This work was supported by National Science Foundation by Award No. NSF CBET 1704668.

[1] L. M. Mashburn and M. Whiteley, Membrane vesicles traffic signals and facilitate group activities in a prokaryote, Nature (London) **437**, 422 (2005).

[2] S. Sowinski, C. Jolly, O. Berninghausen, M. A. Purbhoo, A. Chauveau, K. Köhler, S. Oddos, P. Eissmann, F. M. Brodsky, C. Hopkins *et al.*, Membrane nanotubes physically connect T cells over long distances presenting a novel route for HIV-1 transmission, Nat. Cell Biol. **10**, 211 (2008).

[3] R. Langer, New methods of drug delivery, Science **249**, 1527 (1990).

[4] R. Lipowsky, The conformation of membranes, Nature (London) **349**, 475 (1991).

[5] H. Noguchi and G. Gompper, Shape transitions of fluid vesicles and red blood cells in capillary flows, Proc. Natl. Acad. Sci. USA **102**, 14159 (2005).

[6] D. Boal, *Mechanics of the Cell* (Cambridge University Press, Cambridge, UK, 2002).

[7] S. F. Fenz and K. Sengupta, Giant vesicles as cell models, Integr. Biol. **4**, 982 (2012).

[8] D. Chen and M. M. Santore, Large effect of membrane tension on the fluid–solid phase transitions of two-component phosphatidylcholine vesicles, Proc. Natl. Acad. Sci. USA **111**, 179 (2014).

[9] F. C. Keber, E. Loiseau, T. Sanchez, S. J. DeCamp, L. Giomi, M. J. Bowick, M. C. Marchetti, Z. Dogic, and A. R. Bausch, Topology and dynamics of active nematic vesicles, Science **345**, 1135 (2014).

[10] R. Dimova and C. Marques, *The Giant Vesicle Book* (CRC Press, Boca Raton, FL, 2019).

[11] E. Amstad, J. Kohlbrecher, E. Müller, T. Schweizer, M. Textor, and E. Reimhult, Triggered release from liposomes through magnetic actuation of iron oxide nanoparticle containing membranes, Nano Lett. **11**, 1664 (2011).

[12] A. Jesorka and O. Orwar, Liposomes: Technologies and analytical applications, Annu. Rev. Anal. Chem. **1**, 801 (2008).

[13] C. Misbah, Vacillating Breathing and Tumbling of Vesicles Under Shear Flow, Phys. Rev. Lett. **96**, 028104 (2006).

[14] G. Danker and C. Misbah, Rheology of a Dilute Suspension of Vesicles, Phys. Rev. Lett. **98**, 088104 (2007).

[15] B. Kaoui, G. Biros, and C. Misbah, Why Do Red Blood Cells Have Asymmetric Shapes Even in a Symmetric Flow?, Phys. Rev. Lett. **103**, 188101 (2009).

[16] G. Danker, P. M. Vlahovska, and C. Misbah, Vesicles in Poiseuille Flow, Phys. Rev. Lett. **102**, 148102 (2009).

[17] G. Coupier, A. Farutin, C. Minetti, T. Podgorski, and C. Misbah, Shape Diagram of Vesicles in Poiseuille Flow, Phys. Rev. Lett. **108**, 178106 (2012).

[18] V. Kantsler and V. Steinberg, Transition to Tumbling and Two Regimes of Tumbling Motion of a Vesicle in Shear Flow, Phys. Rev. Lett. **96**, 036001 (2006).

[19] V. Kantsler and V. Steinberg, Orientation and Dynamics of a Vesicle in Tank-Treading Motion in Shear Flow, Phys. Rev. Lett. **95**, 258101 (2005).

[20] V. Kantsler, E. Segre, and V. Steinberg, Critical Dynamics of Vesicle Stretching Transition in Elongational Flow, Phys. Rev. Lett. **101**, 048101 (2008).

[21] V. Kantsler, E. Segre, and V. Steinberg, Vesicle Dynamics in Time-Dependent Elongation Flow: Wrinkling Instability, Phys. Rev. Lett. **99**, 178102 (2007).

[22] J. B. Dahl, V. Narsimhan, B. Gouveia, S. Kumar, E. S. Shaqfeh, and S. J. Muller, Experimental observation of the asymmetric instability of intermediate-reduced-volume vesicles in extensional flow, Soft Matter **12**, 3787 (2016).

[23] D. Kumar, C. M. Richter, and C. M. Schroeder, Conformational dynamics and phase behavior of lipid vesicles in a precisely controlled extensional flow, Soft Matter **16**, 337 (2020).

[24] C. Lin and V. Narsimhan, Shape stability of deflated vesicles in general linear flows, Phys. Rev. Fluids **4**, 123606 (2019).

[25] J. Deschamps, V. Kantsler, and V. Steinberg, Phase Diagram of Single Vesicle Dynamical States in Shear Flow, Phys. Rev. Lett. **102**, 118105 (2009).

[26] V. Narsimhan, A. P. Spann, and E. S. Shaqfeh, The mechanism of shape instability for a vesicle in extensional flow, J. Fluid Mech. **750**, 144 (2014).

[27] V. Narsimhan, A. P. Spann, and E. S. Shaqfeh, Pearling, wrinkling, and buckling of vesicles in elongational flows, J. Fluid Mech. **777**, 1 (2015).

[28] V. V. Lebedev, K. S. Turitsyn, and S. S. Vergeles, Dynamics of Nearly Spherical Vesicles in an External Flow, Phys. Rev. Lett. **99**, 218101 (2007).

[29] H. Zhao and E. S. Shaqfeh, The shape stability of a lipid vesicle in a uniaxial extensional flow, J. Fluid Mech. **719**, 345 (2013).

[30] H. Zhou, B. B. Gabilondo, W. Losert, and W. van de Water, Stretching and relaxation of vesicles, Phys. Rev. E **83**, 011905 (2011).

[31] S.-H. Wu, S. Sankhagowit, R. Biswas, S. Wu, M. L. Povinelli, and N. Malmstadt, Viscoelastic deformation of lipid bilayer vesicles, Soft Matter **11**, 7385 (2015).

[32] I. V. Pivkin and G. E. Karniadakis, Accurate Coarse-Grained Modeling of Red Blood Cells, Phys. Rev. Lett. **101**, 118105 (2008).

[33] M. Yu, R. B. Lira, K. A. Riske, R. Dimova, and H. Lin, Ellipsoidal Relaxation of Deformed Vesicles, Phys. Rev. Lett. **115**, 128303 (2015).

[34] A. Shenoy, C. V. Rao, and C. M. Schroeder, Stokes trap for multiplexed particle manipulation and assembly using fluidics, Proc. Natl. Acad. Sci. USA **113**, 3976 (2016).

[35] D. Kumar, A. Shenoy, S. Li, and C. M. Schroeder, Orientation control and nonlinear trajectory tracking of colloidal particles using microfluidics, Phys. Rev. Fluids **4**, 114203 (2019).

[36] A. Shenoy, D. Kumar, S. Hilgenfeldt, and C. M. Schroeder, Flow topology during multiplexed particle manipulation using a Stokes trap, Phys. Rev. Appl. **12**, 054010 (2019).

[37] D. Kumar, A. Shenoy, J. Deutsch, and C. M. Schroeder, Automation and flow control for particle manipulation, Curr. Opin. Chem. Eng. **29**, 1 (2020).

[38] See Supplemental Material at http://link.aps.org/supplemental/10.1103/PhysRevE.102.010605 for movies, figures, and details of the viscoelastic model.

[39] M. Angelova, S. Soléau, P. Méléard, F. Faucon, and P. Bothorel, Preparation of giant vesicles by external ac electric fields. Kinetics and applications, in *Trends in Colloid and Interface Science VI* (Springer, New York, 1992), pp. 127–131.

[40] J. Pécréaux, H.-G. Döbereiner, J. Prost, J.-F. Joanny, and P. Bassereau, Refined contour analysis of giant unilamellar vesicles, Eur. Phys. J. E **13**, 277 (2004).

[41] H. A. Faizi, C. J. Reeves, V. N. Georgiev, P. M. Vlahovska, and R. Dimova, Fluctuation spectroscopy of giant unilamellar vesicles using confocal and phase contrast microscopy, arXiv:2005.09715.

[42] J.-B. Fournier, A. Ajdari, and L. Peliti, Effective-Area Elasticity and Tension of Micromanipulated Membranes, Phys. Rev. Lett. **86**, 4970 (2001).

[43] R. Dimova, U. Seifert, B. Pouligny, S. Förster, and H.-G. Döbereiner, Hyperviscous diblock copolymer vesicles, Eur. Phys. J. E **7**, 241 (2002).

[44] U. Seifert, Fluid membranes in hydrodynamic flow fields: Formalism and an application to fluctuating quasispherical vesicles in shear flow, Eur. Phys. J. B **8**, 405 (1999).

[45] L. Liu, M. Yu, H. Lin, and R. Foty, Deformation and relaxation of an incompressible viscoelastic body with surface viscoelasticity, J. Mech. Phys. Solids **98**, 309 (2017).

[46] S. T. Milner and S. A. Safran, Dynamical fluctuations of droplet microemulsions and vesicles, Phys. Rev. A **36**, 4371 (1987).

[47] J.-W. Ha and L. G. Leal, An experimental study of drop deformation and breakup in extensional flow at high capillary number, Phys. Fluids **13**, 1568 (2001).

[48] L. Miao, U. Seifert, M. Wortis, and H.-G. Döbereiner, Budding transitions of fluid-bilayer vesicles: The effect of area-difference elasticity, Phys. Rev. E **49**, 5389 (1994).

[49] N. Fa, L. Lins, P. J. Courtoy, Y. Dufrêne, P. Van Der Smissen, R. Brasseur, D. Tyteca, and M.-P. Mingeot-Leclercq, Decrease of elastic moduli of DOPC bilayers induced by a macrolide antibiotic, azithromycin, Biochim. Biophys. Acta **1768**, 1830 (2007).

[50] X. Trepat, L. Deng, S. S. An, D. Navajas, D. J. Tschumperlin, W. T. Gerthoffer, J. P. Butler, and J. J. Fredberg, Universal physical responses to stretch in the living cell, Nature (London) **447**, 592 (2007).

[51] A. Rigato, A. Miyagi, S. Scheuring, and F. Rico, High-frequency microrheology reveals cytoskeleton dynamics in living cells, Nat. Phys. **13**, 771 (2017).

[52] M. Yu, A. Mahtabfar, P. Beelen, Y. Demiryurek, D. I. Shreiber, J. D. Zahn, R. A. Foty, L. Liu, and H. Lin, Coherent timescales and mechanical structure of multicellular aggregates, Biophys. J. **114**, 2703 (2018).

[53] T. G. Mason and D. A. Weitz, Optical Measurements of Frequency-Dependent Linear Viscoelastic Moduli of Complex Fluids, Phys. Rev. Lett. **74**, 1250 (1995).

[54] T. T. Hormel, S. Q. Kurihara, M. K. Brennan, M. C. Wozniak, and R. Parthasarathy, Measuring Lipid Membrane Viscosity Using Rotational and Translational Probe Diffusion, Phys. Rev. Lett. **112**, 188101 (2014).

[55] A. Mietke, O. Otto, S. Girardo, P. Rosendahl, A. Taubenberger, S. Golfier, E. Ulbricht, S. Aland, J. Guck, and E. Fischer-Friedrich, Extracting cell stiffness from real-time deformability cytometry: Ttheory and experiment, Biophys. J. **109**, 2023 (2015).

[56] F. Brochard-Wyart, N. Borghi, D. Cuvelier, and P. Nassoy, Hydrodynamic narrowing of tubes extruded from cells, Proc. Natl. Acad. Sci. USA **103**, 7660 (2006).

[57] O. Rossier, D. Cuvelier, N. Borghi, P. Puech, I. Derényi, A. Buguin, P. Nassoy, and F. Brochard-Wyart, Giant vesicles under flows: Extrusion and retraction of tubes, Langmuir **19**, 575 (2003).